

Investigating the intra-urban urban heat island effect for two subtropical mega-urban regions in China by adopting local climate zone

16

Meng Cai¹, Ran Wang², Chao Ren³ and Edward Ng¹

¹*School of Architecture, The Chinese University of Hong Kong, Hong Kong, PR China;* ²*College of Economic and Social Development, Nankai University, Tianjin, PR China;* ³*Division of Landscape Architecture, Department of Architecture, Faculty of Architecture, The University of Hong Kong, Pokfulam, Hong Kong, PR China*

1. Introduction

The phenomenon that urban temperature is higher than that of its surrounding rural areas, which is called Urban Heat Island (UHI), has been observed and documented worldwide (Clinton and Gong, 2013; Heinel et al., 2015; McCarthy et al., 2010; Oke, 1973; Peng et al., 2011; Santamouris et al., 2015; Zhao et al., 2014). An intensifying UHI effect, which is closely related to surface changes, is seen as an inevitable problem (Mallick et al., 2008). Given the significant urbanization around the world, the surface temperature is expected to keep rising, and an increasing proportion of the worldwide population will be exposed to the rising temperature in urban areas (Allen et al., 2014). Generally, the UHI comprises both air temperature UHI and surface UHI (SUHI), which are defined by (canopy or boundary layer) air temperature and LST differences between urban and rural areas, respectively. Air temperature is measured in situ using station networks. However, the coverage of ground-level observational meteorological stations is limited in China, and air temperature is difficult to acquire in high temporal and spatial resolution. Land surface temperature (LST) measured by thermal infrared radiometers carried by aircraft or satellites can provide continuous coverage, high integrity, and real-time data acquisition over large areas (Voogt and Oke, 2003).

Scholars have investigated the changes of land covers, LST, and SUHI effect as well as their relationship (Qian and Ding, 2005; Weng, 2001). However, most studies adopt a rough urban classification scheme with commonly one urban category (Tian et al., 2017). Such a single urban classification system ignores the complexity and spatial heterogeneity of urban structure. Detailed urban categories will help develop an in-depth understanding of the spatial variations of the local climate, as well as the relationship between land cover and the magnitude of the SUHI. To ensure effective and coherent development of adaptation strategies aimed at improving the urban thermal environment, it is

necessary to utilize a uniform urban classification scheme for the understanding of the intraurban UHI and the impact of urban land cover.

The World Urban Database and Access Portal Tools (WUDAPT) was developed as a new global initiative to produce standardized data on urban form and function for different applications and in different levels of detail (Bechtel et al., 2015; Ching et al., 2018). This most basic description of urban landscapes in WUDAPT (= level zero) (Bechtel et al., 2019) discretizes urban landscapes into Local Climate Zones (LCZs), a scheme that comprises 10 built types and seven land cover types (Table 16.1) (Stewart and Oke, 2012). With the 10 built types, the intraurban structure can be investigated in sufficient detail for many climatic applications. Moreover, LCZ links land cover types and urban morphology with corresponding thermal properties, which is particularly suitable as a standardized method for intraurban UHI investigations across different cities and regions (Stewart and Oke, 2012).

WUDAPT suggests a standardized workflow to generate LCZ maps representing different built and natural land cover types (Bechtel et al., 2015). It contains three major steps: Firstly, the preprocessing of Landsat images: Landsat images were mosaicked into one image to cover the study area. Next, this image was resampled from 30 to 100 m resolution and clipped to fit the range of the region. Secondly, selection of training samples: polygons, representing training samples for all LCZ types present, were digitized from Google Earth based on local knowledge. Thirdly, LCZ classification by the random forest classifier: the preprocessed Landsat images and selected training samples were used to train a random forest classifier (Breiman, 2001). Taking advantage of spectral features contained in each training sample, the random forest classifier generated the classification rule and applied it to identify each pixel. The random classifier was selected as an ideal compromise between the achieved accuracy and computational performance among the previously tested classifiers (Bechtel and Daneke, 2012).

As a consequence of the opening and reform policy since 1978, China is experiencing rapid growth in both the number of megaurban regions and their population (Tan, 20107). The central government of China regards megaurban region development strategy as a principal urbanization platform in 2014 (CCCPC and SC, 2014). Yangtze River Delta (YRD) and Pearl River Delta (PRD) regions are two leading subtropical megaurban regions experiencing rapid urban expansion and warming land surface. In this context, it is imperative to understand the spatial patterns of the UHI and propose UHI mitigation strategies for the two regions. Thus, this study applied the LCZ-based WUDAPT data and LST to analyze the intraurban UHI in the YRD and PRD regions.

2. Case study: Pearl River Delta region

2.1 Location and urbanization of the PRD

The PRD region is located in the Guangdong province, in the southeast of China, close to the South China Sea (Fig. 16.1). The PRD region covers an area of 55,000 km². It used to be a major agricultural production area before the implementation of the opening and reform policy in 1978. In the 1980s, the name “Pearl River Delta (PRD) region” was put forward as an economic and industrial region. After the putting forward of the opening and reform policy, with the increasing prosperity of different industries, a large population of workers and new immigrants moved into this region. Correspondingly, a large amount of agricultural land was converted into construction land to support economic growth and building construction for urban dwellers. From 2000 to 2010, the urban area in the PRD region grew by 2615 km² (Statistics Bureau of Guangdong Province, 2001, 2011). In 2008, the urbanization rate of the

Table 16.1 Snapshots of different LCZ classes in the YRD megaurban region from Google Earth.**LCZ 1: Compact high-rise**

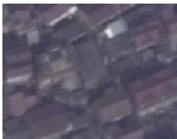
- Tightly packed buildings with more than 10 stories
- Little or no green space
- Built by concrete, steel, stone, and glass

**LCZ 4: Open high-rise**

- Openly arranged buildings with more than 10 stories
- Abundance green space
- Built by concrete, steel, stone, and glass

**LCZ 7: Lightweight low-rise**

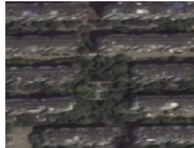
- Lightweight building materials with one to two stories
- Few or no trees
- Land cover is hard-packed

**LCZ 2: Compact mid-rise**

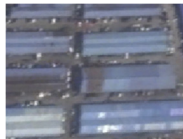
- Tightly packed buildings with three to nine stories
- Little or no green space
- Built by stone, brick, tile, and concrete

**LCZ 5: Open mid-rise**

- Openly arranged buildings with three to nine stories
- An abundance of green space
- Built by concrete, steel, and glass

**LCZ 8: Large low-rise**

- Large, openly arranged buildings with one to three stories
- Few green spaces
- Land cover is mostly paved

**LCZ 3: Compact low-rise**

- Tightly packed buildings with one to three stories
- Little or no green space
- Built by concrete, steel, stone, and glass

**LCZ 6: Open low-rise**

- Openly arranged buildings with one to three stories
- An abundance of green space
- Built by wood, brick, tile, and concrete

**LCZ 9: Sparsely built**

- Sparse arrangement of small or medium-sized buildings in a natural setting
- An abundance of pervious cover

*Continued*

Table 16.1 Snapshots of different LCZ classes in the YRD megaurban region from Google Earth.—cont'd

LCZ 10: Heavy industry

- Low-rise and mid-rise industrial structures (towers, tanks, stacks)
- Few or no trees



LCZ C: Bush, scrub

- Open arrangement of bushes, shrubs, and short, woody trees



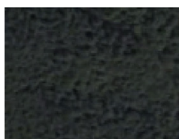
LCZ F: Bare soil or sand

- Soil or sand cover



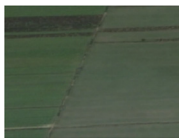
LCZ A: Dense trees

- The heavily wooded landscape of deciduous and/or evergreen trees



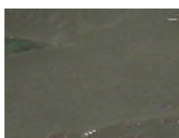
LCZ D: Low plants

- Grass or herbaceous plants/crops



LCZ G: Water

- Large, open water bodies



LCZ B: Scattered trees

- The lightly wooded landscape of deciduous and/or evergreen trees



LCZ E: Bare rock or paved

- Rock or paved cover



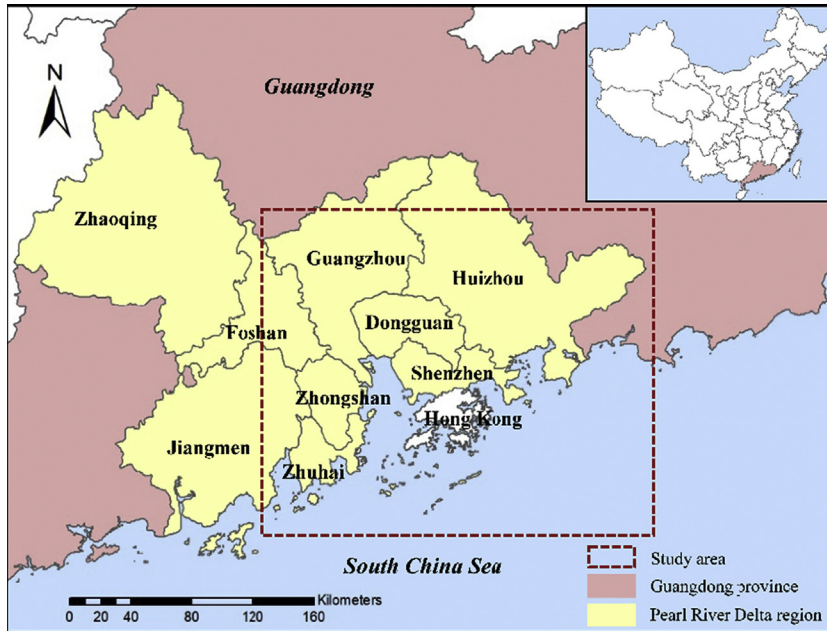


FIGURE 16.1

Location and main cities of the Pearl River Delta (PRD) region.

PRD region was up to 80.5%, and the built-up areas took up around 16% of the whole area of the PRD region (Government of Guangdong Province, 2010). This leads to rapid land cover change with urban development, a problem that is not unique to the PRD region, since many cities or regions within fast urban development in China. And other fast-developing countries are facing similar problems (Lambin, 1997; Murdiyarso, 2000).

2.2 Land cover change in the PRD

The LCZ maps of the PRD region for 1999, 2009, and 2014 are shown in Fig. 16.2. Accuracy assessment is conducted based on three sets of independent validation samples, which were depicted using Google Earth. The overall accuracies for the LCZ maps of 1999, 2009, and 2014 are 73%, 71%, 76% and the Kappa coefficients for the three maps are 0.70, 0.68, and 0.73. Qualitatively, it is found that the built-up areas in the PRD region kept on enlarging from 1999 to 2014.

Table 16.2 illustrates the quantitative change of each LCZ type in the PRD region from 1999 to 2014. The results show that the percentage of compact LCZs (LCZ 1–3) keeps rising; while the percentage of open LCZs (LCZ 4–6) decreases slightly between 1999 and 2014. The area of LCZ 7 (lightweight low-rise), most of which are rural villages, reduced over the entire period. The extent of the most natural land cover types, namely LCZ A–G, was reduced during the study period.

As shown in Tables 16.3 and 16.4, the areas of LCZ built types (LCZ 1–10) increased with a faster increasing rate during subperiod 1 (1999–2009). The area of compact LCZ types (LCZ 1–3)

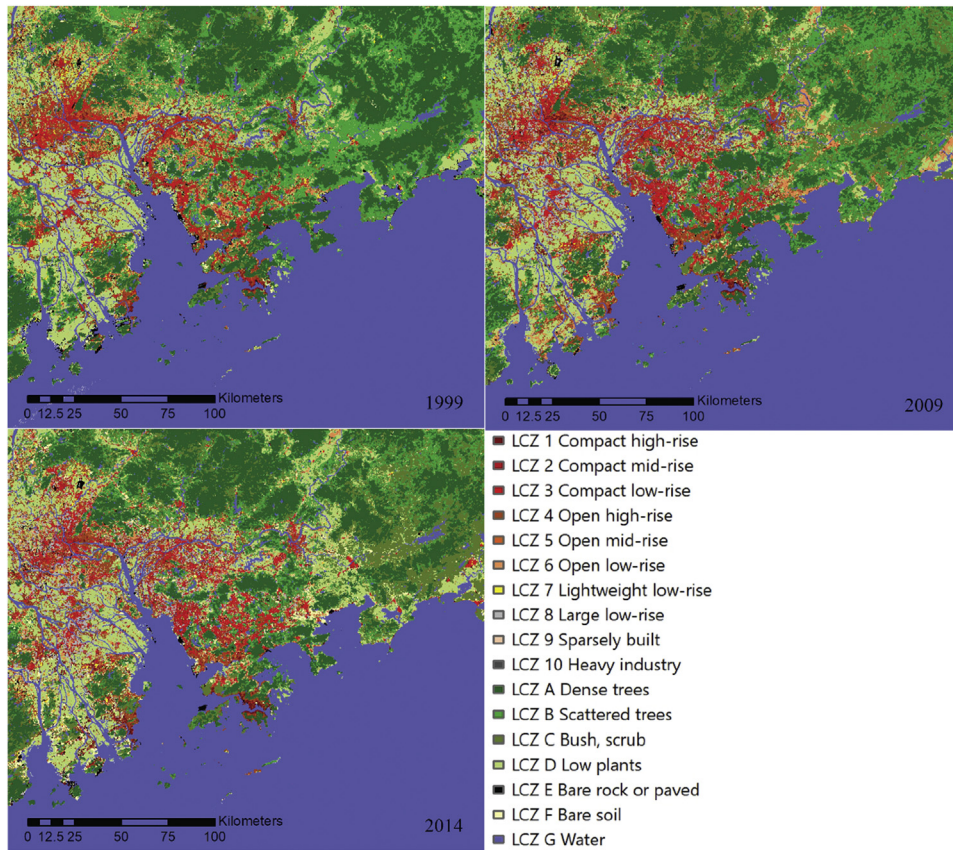


FIGURE 16.2

LCZ maps of the PRD region in the year of 1999, 2009, and 2014.

increased mainly due to the transformation from other built types (e.g., open LCZs) and transformation from natural LCZ types, especially LCZ B (scattered trees) and LCZ D (low plants), illustrating both densification and vertical enhancement in the PRD region.

For natural LCZ types, transformations mainly occurred between different land covers and from land cover types to built types. LCZ A (dense trees), LCZ B (scattered trees), LCZ C (bush, scrub), and LCZ D (low plants) converted to each other. Noticeably, the area of LCZ A (dense trees) decreased by 2386 km² with nearly no incoming sources from other LCZ classes during subperiod 1. While LCZ A and LCZ D both gained areas from LCZ B and LCZ C during subperiod 2 (2009–14). For LCZ E (bare rock/paved) and LCZ F (bare soil), both areas decreased during subperiod 1, respectively; but increased during subperiod 2. While the area of LCZ G (water bodies) remained stable with mere changes of 2 km².

Table 16.2 Share of the LCZ types in the PRD region from 1999 to 2014 (%).

Year	1	2	3	4	5	6	7	8	9	10	A	B	C	D	E	F	G
1999	0.21	0.41	1.78	4.87	0.23	2.30	0.52	0.49	0.05	0.12	17.54	11.58	3.23	10.26	0.86	0.57	45.00
2009	0.48	0.32	2.51	6.42	0.16	2.08	0.28	1.92	0.12	0.15	13.38	8.79	8.55	9.41	0.31	0.14	45.00
2014	0.51	0.76	2.70	4.80	0.10	2.06	0.38	2.07	0.22	0.13	14.30	6.51	8.45	9.96	0.43	1.61	45.00

Table 16.3 Land cover transformation matrix of the PRD region from 1999 to 2009 (km²).

LCZ class ^a		2009																Sum (1999)	
		1	2	3	4	5	6	7	8	9	10	A	B	C	D	E	F		G
1999	1	50	2	13	22	0	8	0	10	1	1	0	1	1	7	1	1	0	120
	2	47	55	85	21	4	2	2	17	0	1	0	0	0	1	1	0	0	237
	3	28	76	599	67	5	44	30	132	1	7	0	1	3	25	5	0	0	1024
	4	40	26	354	1505	27	190	31	322	4	22	7	14	13	216	17	6	0	2795
	5	15	8	14	36	43	4	2	4	0	0	1	0	0	3	0	0	0	130
	6	9	5	136	451	2	210	8	175	18	5	5	51	72	135	26	14	0	1320
	7	2	2	72	39	2	32	68	12	0	0	6	13	7	44	1	0	0	300
	8	2	0	11	43	1	5	1	160	0	0	0	1	2	36	1	0	16	279
	9	0	0	0	4	0	3	0	0	6	0	5	3	4	2	0	0	0	28
	10	1	0	3	18	0	9	0	6	0	19	0	0	1	4	4	0	1	67
	A	3	0	2	94	4	30	0	6	11	1	6701	2058	990	155	7	4	3	10,068
	B	19	1	37	421	1	191	3	85	15	3	491	2392	2318	620	25	22	0	6645
	C	1	0	1	31	0	12	0	3	5	1	362	320	1062	48	2	3	0	1853
	D	47	6	99	742	3	420	12	128	4	10	44	114	342	3881	22	11	1	5888
	E	6	2	12	132	1	24	1	34	0	5	9	11	26	173	56	4	0	496
	F	2	0	2	57	0	11	0	7	1	0	49	63	67	47	5	15	0	326
	G	0	0	0	0	0	0	0	0	0	10	0	1	1	5	3	0	25,811	25,832
	Sum (2009)	273	186	1440	3684	92	1196	158	1100	66	86	7682	5044	4908	5403	175	80	25,834	

^aRows indicate LCZ types in 1999; columns indicate LCZ types in 2009.

Table 16.4 Land cover transformation matrix of the PRD region from 2009 to 2014 (km²).

LCZ class ^a		2014																	
		1	2	3	4	5	6	7	8	9	10	A	B	C	D	E	F	G	Sum (2009)
2009	1	75	19	16	86	1	5	1	12	0	1	0	1	2	24	4	25	0	273
	2	5	80	54	17	2	3	1	14	0	2	0	0	0	0	6	1	0	186
	3	16	186	841	81	4	46	50	168	2	7	1	5	1	12	13	8	0	1440
	4	110	78	226	1653	18	352	26	195	19	19	37	214	42	466	39	190	0	3684
	5	1	8	5	35	17	15	1	1	0	0	1	2	2	2	1	0	0	92
	6	11	20	112	103	6	289	38	34	13	3	9	57	54	297	31	118	0	1196
	7	1	8	45	10	2	16	62	4	0	0	0	1	1	5	2	2	0	158
	8	12	25	190	80	2	36	3	653	2	9	3	11	3	25	23	21	0	1100
	9	0	0	1	7	0	9	0	1	15	0	5	17	5	4	0	1	0	66
	10	5	2	5	4	0	2	0	18	0	21	0	1	1	1	16	6	4	86
	A	1	0	1	52	0	10	0	2	10	0	6163	591	679	141	2	30	0	7682
	B	1	1	5	78	1	34	2	6	18	1	1143	1538	1567	539	5	105	1	5044
	C	2	1	5	80	0	45	2	7	21	1	757	992	2248	607	4	136	1	4908
	D	42	9	34	451	5	305	26	51	24	6	82	302	237	3572	31	221	5	5403
	E	3	3	8	11	0	8	1	19	0	3	3	2	5	14	64	29	1	175
	F	2	1	2	8	0	5	0	5	0	1	1	7	4	10	4	31	0	80
G	2	0	0	1	0	0	0	0	0	0	4	0	1	0	4	1	25,821	25,834	
Sum (2014)	290	439	1549	2757	59	1181	216	1190	125	75	8210	3739	4851	5718	249	926	25,834		

^aRows indicate LCZ types in 2009; columns indicate LCZ types in 2014.

From the above two tables, the urbanization in the PRD region showed a continuous conversion from natural to urban LCZ types, but also densification as well as vertical enhancement of existing urban structures. All three processes can be seen in the multitemporal LCZ mapping.

2.3 Land surface temperature analysis in the PRD

LST of the PRD region during both the day and night from June to September was retrieved from MODIS image in 2000, 2009, and 2015. [Table 16.5](#) shows the patterns of LST in the PRD region in 2000, 2009, and 2015, respectively. In general, the higher LST is located in the built-up areas, mainly compromised of the downtown areas of Guangzhou, Dongguan, Foshan, Shenzhen, Hong Kong, Zhuhai, and Macao. Besides, there is no apparent gap of the warmer surface (identified as red in the images) among different cities, indicating that the urbanization has led to the built-up areas in different cities merged into one large area.

For the daytime images, there is a significant expansion of areas of high LST value along the coast of Guangzhou, Hong Kong, Macao, Shenzhen, and Zhuhai. Furthermore, significant growth of LST heat intensity is captured from the LST images, and the urban areas in 2015 has reached the highest LST in comparison to 2000 and 2009, which may indicate a poor thermal environment in the red areas.

For the nighttime situation, the areas with high LST value are not noticeably detected in 2000. However, the nighttime image in 2009 identified an obvious increase of LST magnitude in the whole region. The area of high LST value also has a large expansion in comparison with the LST in 2000. Also, the nighttime LST pattern is different from that of daytime. Higher LST is more significant in the west of the urban areas such as Guangzhou, Foshan, and Zhuhai. The nighttime LST pattern in 2015 is similar to that of 2009 during the second period.

Here, hot days are defined as days with a maximum temperature of 33°C or above ([Hong Kong Observatory, 2015](#)). Hot nights are not detected based on the LST maps of the region. Only several isolated very hot day spots are identified in 2000 while the expansion of extremely hot weather grows significantly in the region, especially in the downtown areas of the PRD region. The northeast of the PRD region with less urbanization is also under the great potential of extreme heat according to the map. The excessive hot weather may lead to serious health-related impacts to the public in the identified areas.

The mean and standard deviation (SD) of LST for 2000, 2009, and 2015 and the corresponding LST differences are listed in [Table 16.6](#). The average summer LST and SD kept growing during the two subperiods. From 2000 to 2009, the average LST increased by 1.39 and 1.28°C for daytime and nighttime. The SD increased from 1.74 to 1.99 during daytime and from 1.39 to 1.56 in the nighttime. During the second subperiod of 2000–2015, the mean summer LST growth was 0.73 and 0.15°C for daytime and nighttime, respectively. The SD also rose from 1.99 to 2.44 in the daytime and from 1.56 to 1.63 during nighttime during the second subperiod. LST in the daytime situation has a larger increase in LST and LST variations in comparison with nighttime LST.

However, the changes reported in [Table 16.6](#) represent only discrete points in time, and analysis of the LST data each year during the whole period showed that there is substantial interannual variation in summer LST. Therefore, trends for the full period were computed as well.

2.4 Relation of surface warming trend to land cover changes

The land cover changes over the period from 1999 to 2014 in the PRD region were compared to LST trends. First, these trends were calculated based on the summer average (using all valid acquisitions from June to September) of the daily MODIS data for each year from 2000 to 2017. Then linear trends were derived from the time series of annual summer means. Fig. 16.3 indicates significant LST warming with positive trends of up to >0.3 K/year for some parts of the PRD region. Only for a few small parts, negative trends are found, gray areas indicate no significant trends at $P < .05$. Second, the land cover changes in the PRD region based on historical LCZ maps were reclassified as urbanization (natural turning to built LCZ type), deconstruction (vice versa), statically built (same built class in 1999 and 2014), conversion (change within built type), and natural/water (natural class without conversion). Fig. 16.4 shows the land cover changes in the PRD region from 1999 to 2014. Finally, a visual comparison was conducted between the LST trends and land cover changes of the PRD region. Both maps match closely, revealing great spatial accordance between the urbanization and conversion (often related to densification or height enhancement) in Fig. 16.4 and the great LST warming in Fig. 16.3. Thus, qualitatively, the LST changes echo the land cover changes in the PRD region during the study period and most likely dominantly result from the land cover change.

2.5 Thermal characteristic of LCZ type

To analyze the influence of land cover change on LST, the LST in each LCZ was calculated for daytime and nighttime (Fig. 16.5). It is noted that the mean LST of built types is higher than that of natural LCZ types. Among built types, LCZ 2 (compact mid-rise), 8 (large low-rise), and 10 (heavy industry) have the highest LST values at both daytime and nighttime. For natural cover types, LCZ A (dense trees), LCZ B (scattered trees), and LCZ C (bush, scrub) show relatively low mean LST values among all 17 LCZ classes. In addition, variations within the same LCZ class are higher in the daytime than at nighttime.

LSTs of the majority of the LCZ classes have increased during the two periods, indicating an overall trend of surface warming across the study area. However, it also could be related to conversion within one LCZ class or of adjacent patches, since the coarser MODIS data necessarily integrate over somewhat larger areas. In particular, the transformation between different LCZ types (especially urban expansion) has intensified the UHI effect by increasing the LST in the built-up LCZ classes (see Fig. 16.3). The only LST decrease is identified in LCZ B (scattered trees) from 2000 to 2009. Also, there is a greater increase in the first period than that in the second period.

2.6 Dominant LCZ type in SUHI zones

The LSTs have been categorized into SUHI zones, and the dominant LCZ type in the SUHI zone has been identified and summarized in Table 16.7. The low and medium SUHI zones with lower LST are dominated by vegetation and water, i.e., LCZ A (dense trees), LCZ D (low plants). These LCZ types with medium and low SUHI were constant during the 15 years in general, which can result from the low LST and the large areas of these classes.

The high SUHI zone caused by the urbanization process is mainly comprised of two built LCZ types, LCZ 4 (open high-rise) and LCZ 8 (large low-rise), which have large coverage and relatively

Table 16.5 LST in the PRD region in 2000, 2009, and 2015.

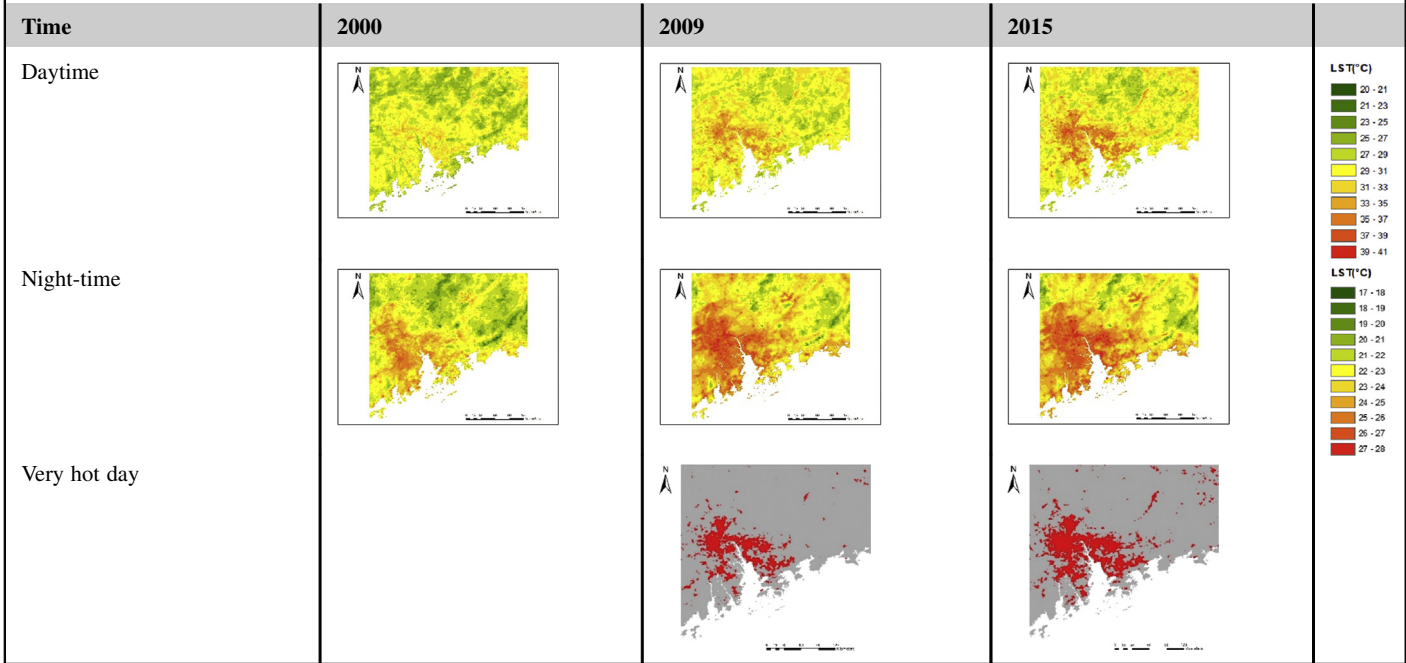
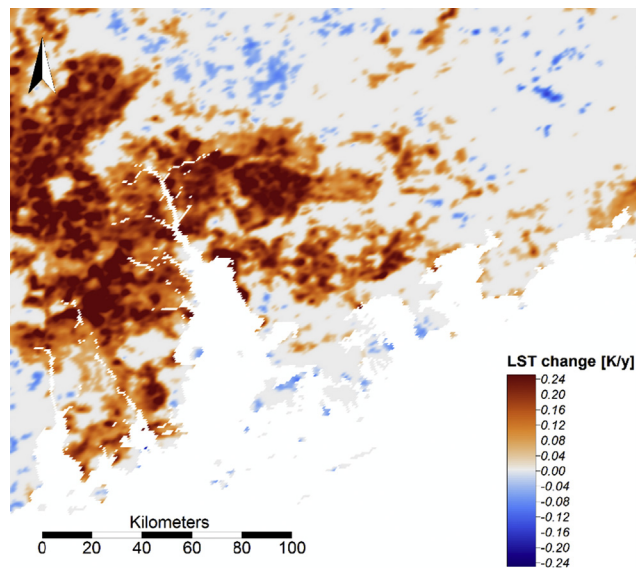


Table 16.6 Mean LST, the LST difference, and standard deviation of LST in 2000, 2009, and 2015 in the PRD region (°C).

	2000	2009	2015
Average daytime summer LST	29.31	30.70	31.43
Average night summer LST	22.94	24.22	24.37
The standard deviation of daytime summer LST	1.74	1.99	2.44
The standard deviation of night summer LST	1.39	1.56	1.63

**FIGURE 16.3**

LST changes from 2000 to 2017 in the PRD region. Gray areas have no significant trends at $P < .05$ confidence level.

higher LST among the built types. LCZ 4 (open high-rise) is the principal LCZ type in high SUHI zones in the daytime. The prevailing LCZ type in high SUHI zones in the night has been changed from LCZ 4 (open high-rise) to LCZ 8 (large low-rise) in 2009. The increase of the area of LCZ 8 (large low-rise), which mainly belongs to manufacturing buildings, can lead to the increase of the LCZ type in the high SUHI zone. The rapid industrial and urbanization process, which can transform land cover types to manufacturing buildings, can aggravate the SUHI effect in the PRD region in the future. In addition, the construction of increasing LCZ 4 (open high-rise) can also intensify the SUHI effect in the PRD region.

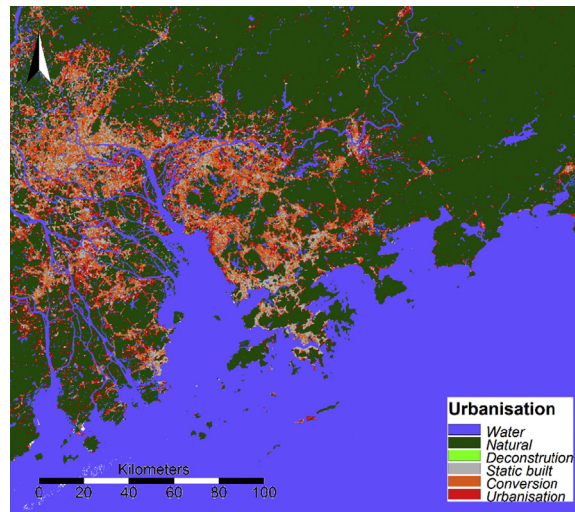


FIGURE 16.4

Land cover changes from 1999 to 2014 in the PRD region.

2.7 Implications for urban planning

LCZ data produced by WUDAPT are further shown to be effectively and efficiently integrated with land cover change and LST analysis in this study. The spatiotemporal distribution of LCZ can be used for land cover change analysis and LST studies, which are beneficial for understanding urban development, land use planning as well as the thermal environment to minimize the negative impact of urbanization. Rapid urban construction has led to the deterioration of the urban thermal environment; hot spots expanded from several cities into merging city groups. Apart from the positive influence of city group mode on urban development, its adverse impact on the urban thermal environment should also be taken into account, especially for regional planning, such as “The PRD Reform and Development Plan (2008–20).” This plan aims to improve the quality of town planning and the management of local urban development through three key aspects: “optimizing spatial plan via making appropriate land use zonings,” “making intensive land use development,” and also “conducting environment protection for sustainable development” (National Development and Reform Commission, 2016). Regarding LCZ classes, in the study period, compact LCZs (LCZ 1–3) were mainly converted from open LCZ types and natural cover types. LCZs with low building height tend to rebuild as LCZ classes with higher heights during the urbanization process. When looking into the thermal environment, LCZ 8 (large low-rise) has the largest increase of LST at daytime, and LCZ 1 (compact high-rise) and LCZ 6 (open low-rise) are the two with the largest increase at nighttime (Appendix.4). LCZ 4 (open high-rise) and LCZ 8 (large low-rise) also contributed largely to the SUHI in the PRD region. The areas of LCZ 1 (compact high-rise) LCZ 4 (open high-rise), and LCZ 8 (large low-rise) also rose dramatically during

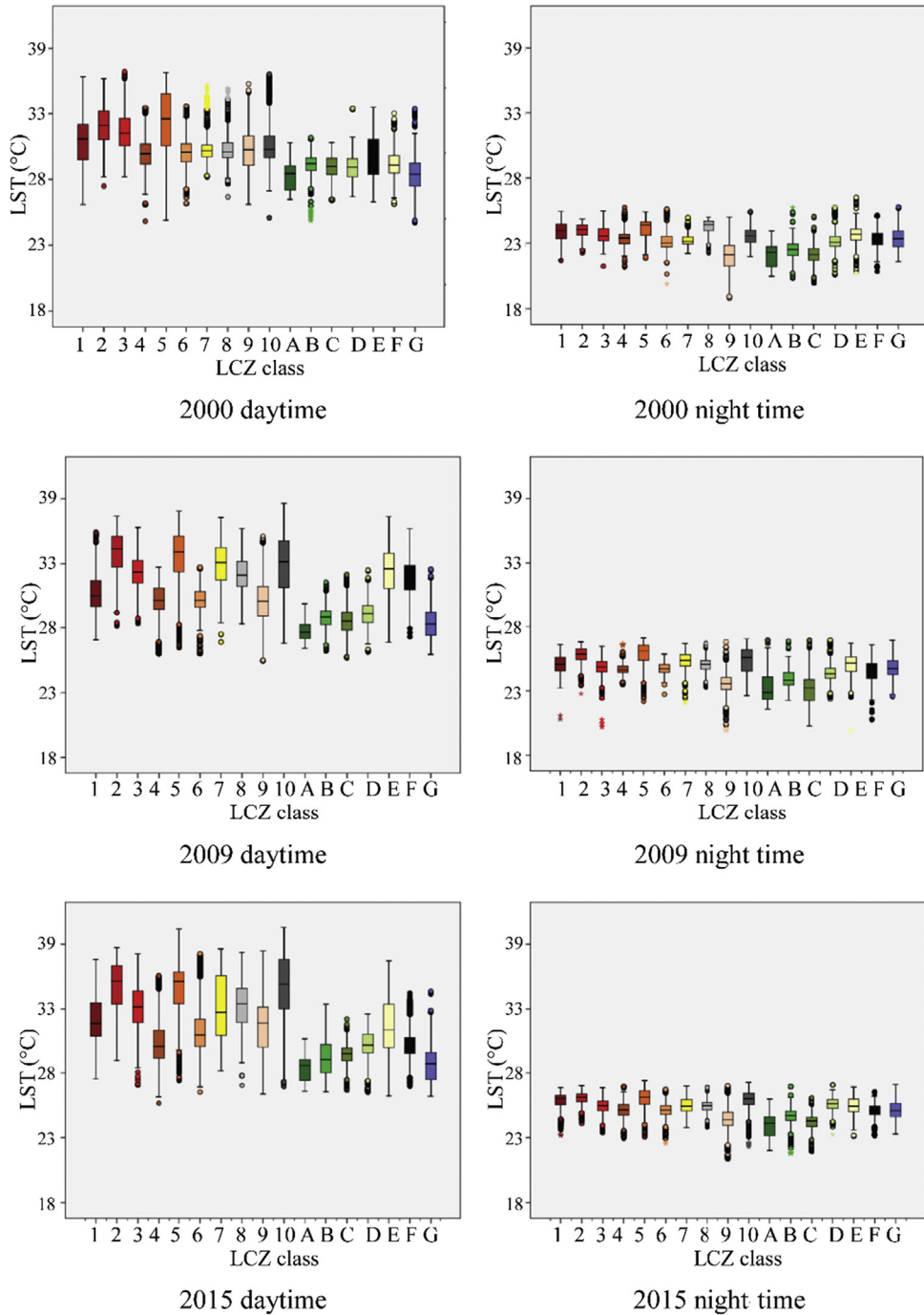


FIGURE 16.5

LST of each LCZ class during daytime and nighttime in 2000, 2009, and 2015.

Table 16.7 Dominant LCZ type in SUHI.

Year	Time	Low SUHI	Medium SUHI	High SUHI
2000	Daytime	LCZ D (low plants)	LCZ G (water)	LCZ 4 (open high-rise)
	Nighttime	LCZ A (dense trees)	LCZ A (dense trees)	LCZ 4 (open high-rise)
2009	Daytime	LCZ A (dense trees)	LCZ A (dense trees)	LCZ 4 (open high-rise)
	Nighttime	LCZ A (dense trees)	LCZ A (dense trees)	LCZ 8 (large low-rise)
2015	Daytime	LCZ A (dense trees)	LCZ A (dense trees)	LCZ 4 (open high-rise)
	Nighttime	LCZ A (dense trees)	LCZ A (dense trees)	LCZ 8 (large low-rise)

this period. Thus, when implementing urban planning for central areas of this megaurban region, compact LCZ types, particularly compact high-rise types, should be paid more attention, since this type has more impact on the thermal environment. The areas of LCZ 4 (open high-rise) and LCZ 8 (large low-rise) should also be restricted with a proper greenery plan in between.

3. Case study: Yangtze River Delta

3.1 Location and urbanization of the YRD

The YRD region is composed of the territory of Shanghai, southern Jiangsu Province, and northern Zhejiang Province (Fig. 16.6). The terrain of this region is generally flat and low-lying floodplain with some hilly areas located in the south of Hangzhou. The YRD region has a subtropical monsoon climate with an annual mean temperature of 15–16°C and annual precipitation of 1000–1,400 mm. Rapid urbanization in this region has given rise to one of the largest megalopolis in the world, covering an area of 99,600 km² and home to over the 83 million urban population (National Development and Reform Commission, 2016). This region is selected in the present paper due to the similar geographic characteristics and urban morphology of the YRD cities.

Two typical cities in the YRD megaurban region under rapid urban development were selected as case studies, namely Shanghai and Hangzhou. Shanghai is located in the center of the alluvial terrace of the Yangtze River delta. It has the highest population density in China and is one of the most vigorous economic zones in the world (Shanghai Municipal Statistics Bureau, 2011). It is divided into 18 county-level divisions with nine districts in the city core collectively identified as urban areas. Hangzhou is the capital of the Zhejiang Province and has the highest population in the province. It is located in the southern part of the YRD and now one of China's most prosperous major cities. Hangzhou municipality area includes nine urban districts, two county-level cities, and two counties.

Previous studies showed that there is a significant UHI phenomenon in the YRD region, characterized by more hot days, higher maximum air temperature, and longer duration of high temperature in urban areas than outer suburbs and periurban areas (Wang and Zheng, 2013; Zhang et al., 2013). UHI intensity in the YRD region reaches 4.7°C (Dong et al., 2014), and the areas experiencing intense UHI have rapidly expanded. In particular, the average UHI intensity in Shanghai reaches 2.4°C in summer (Ding et al., 2014) while the maximum UHI intensity reaches 5.6°C in Hangzhou (Wang and Liu, 1982).

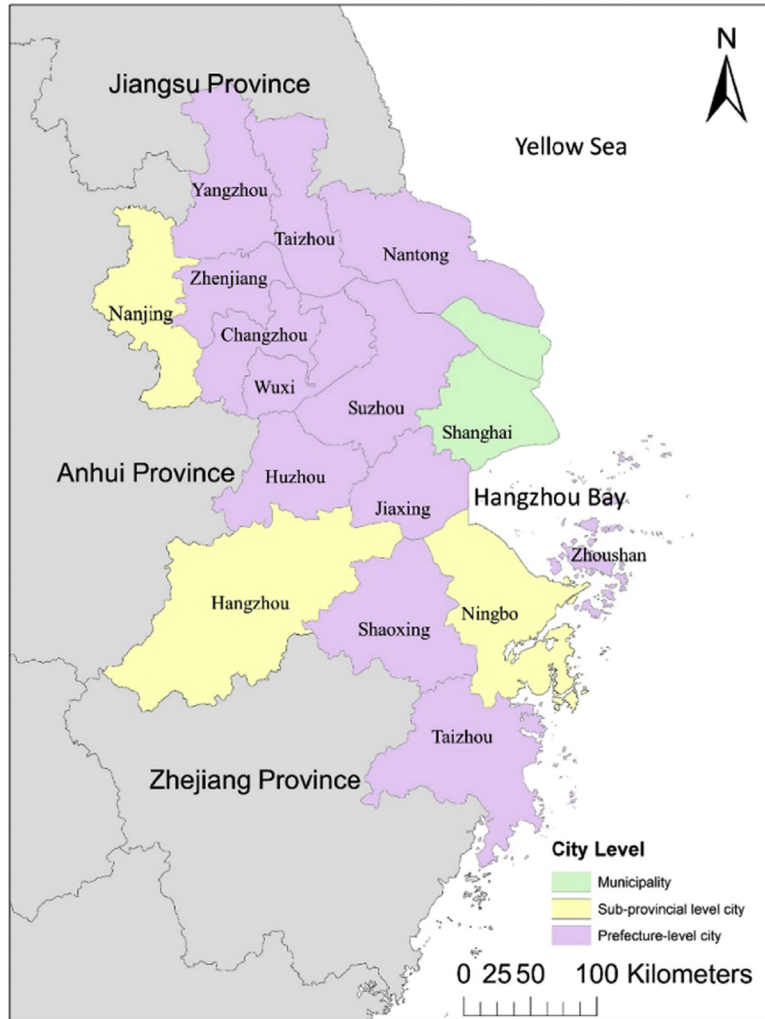


FIGURE 16.6

Location of the study area.

3.2 LCZ maps of the YRD region

Fig. 16.7 is the LCZ map of the YRD megaurban region produced by the improved WUDAPT method. It captures the morphological characteristics of both rural and urban areas and detects the spatial pattern of the potential UHI phenomenon. As shown in Fig. 16.7, the vegetation in the central and northern YRD is dominated by farmland (LCZ D) while the southern and southwestern parts of the

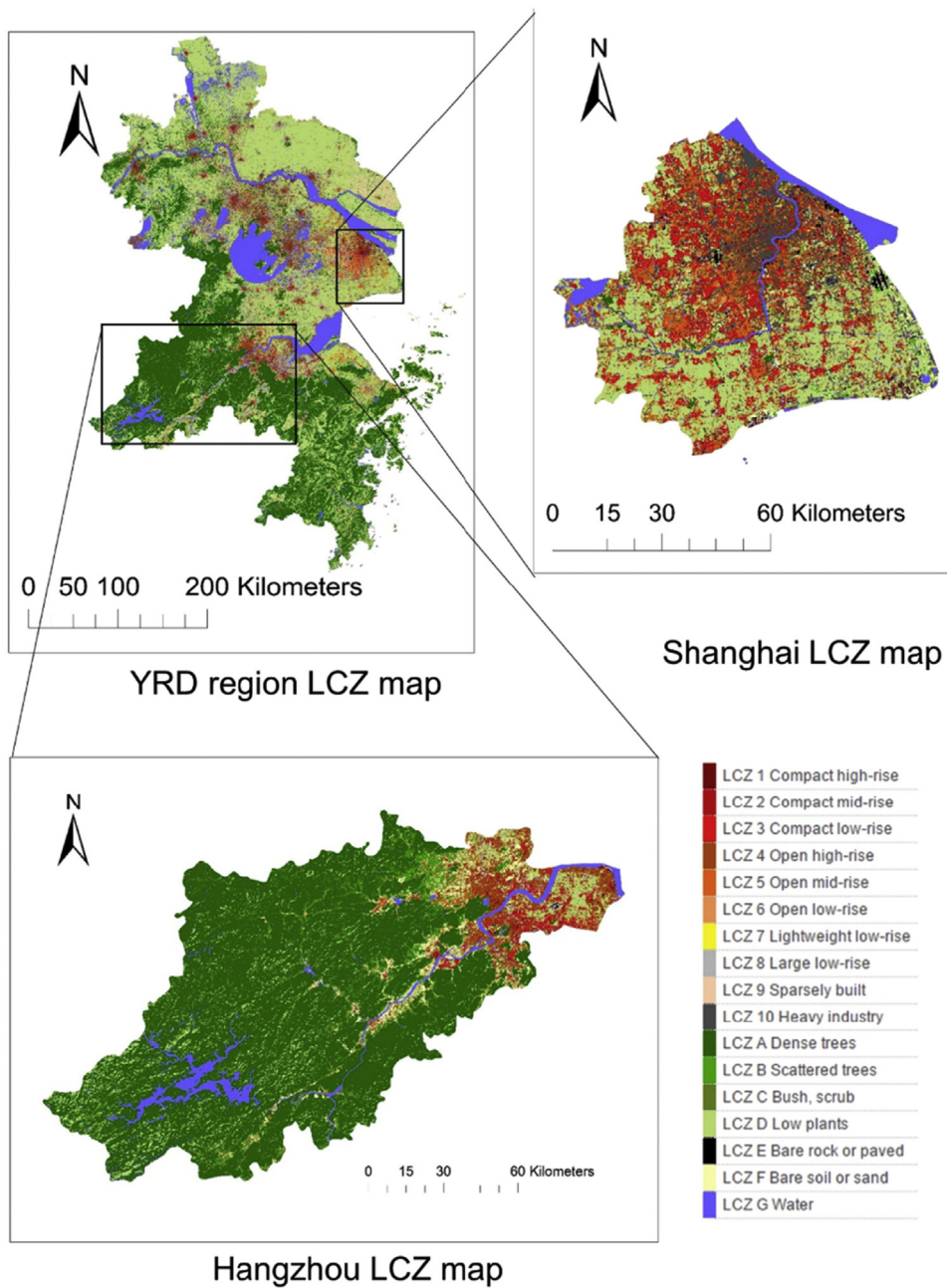


FIGURE 16.7

LCZ maps in the YRD megarban region.

YRD megaurban region are mainly mixed forestland. The vegetation pattern is consistent with the geographic characteristics of the YRD with a low-lying alluvial floodplain in the northern half of the YRD and mountainous terrain in the southwest.

Shanghai has the largest urban areas among all the YRD cities according to the LCZ map. The urban areas have expanded to adjacent cities, namely Suzhou, Wuxi, and Changzhou. These four cities have been integrated into a large city group with no obvious nonurban areas between the cities. Large urban areas are also identified in the two subprovincial-level cities, Hangzhou and Nanjing. There are also many isolated urban settlements in the northern part of YRD, which are mainly suburbs and prefecture-level cities that are possible heat sources of the YRD region.

Downtown areas of Shanghai Municipality, especially in the city center where the CBDs and commercial areas are situated, are extremely dense and compact so they are mainly classified into the LCZ 1–4, which are potential of high UHI intensity. Compact urban land cover is also found in the northern suburbs. Also, the LCZ map detects LCZ 10 (heavy industry) in Baoshan district in the north and Minhang district in the middle of Shanghai that are sources of anthropogenic heat.

The LCZ map of Hangzhou indicates that LCZ A (dense trees) occupies most of the rural areas in the mountain region. Urban settlements are concentrated in the northeastern downtown area. They are not as dense as Shanghai since mainly LCZ 2–5 are found in this region where the UHI phenomenon possibly occurs. In addition, the continuously connected downtown area and suburbs indicate potential aggregation of the UHI phenomenon in Hangzhou. The rest of the counties and county-level cities are mostly classified into LCZ 3 (compact low-rise).

In addition, there are misclassifications in vegetation covers such as LCZ B and C since it is difficult for the random forest classifier to distinguish vegetation with various heights and densities. It is also because the satellite imagery does not contain sufficient information about the height and density of vegetation. On the other hand, the misclassification results from the inconsistent dates of the images obtained from Google Earth and Landsat data since the density and height of vegetation may vary across different seasons. Therefore, multitemporal Landsat images are required to provide more accurate results.

3.3 SUHI intensity in the YRD

The SUHI of Shanghai and Hangzhou was classified according to (Zhang et al., 2013). Fig. 16.8 shows the spatial pattern of surface UHI classified in Shanghai and Hangzhou based on the LST acquired from night-time Aster thermal images. In Shanghai, the SUHI intensity reaches up to 4.2°C in downtown areas in the center and northern part of Shanghai. High LST was extensively found in the southern suburbs while scattered, extremely high LST values were observed outside the city center due to the presence of point sources such as the factories in the north of Baoshan and the south of Minhang. It is also notable that the distribution of high LST is dominant in the city.

SUHI is more prominent in Hangzhou with a large area of high LST found in the downtown area in the northwestern part of the city. The temperature difference between the downtown and surrounding rural areas reaches up to 12°C in LST. In particular, Hangzhou Bay in the southeast has a SUHI intensity of 10°C since it is an economic development zone surrounded by Hangzhou, Shanghai, and Ningbo, leading to such the prominence of SUHI in this area.

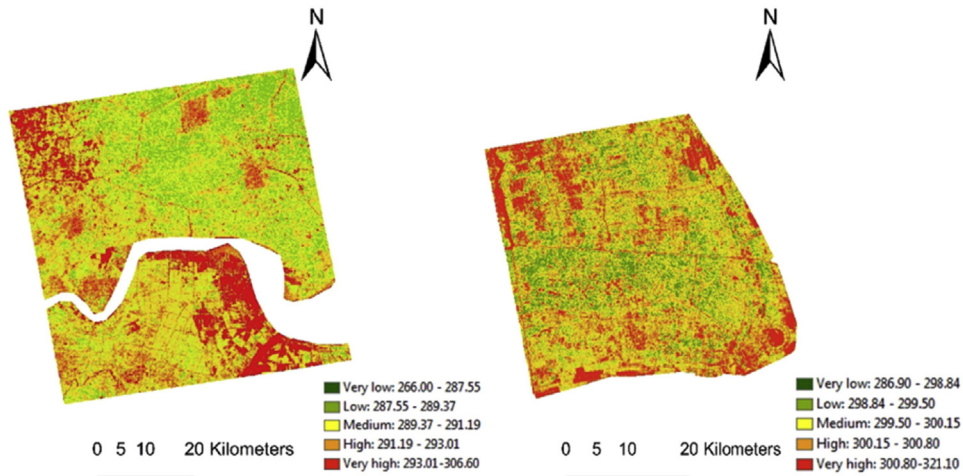


FIGURE 16.8

Spatial variation of surface UHI in Shanghai (left) and Hangzhou (right).

3.4 Relationship between surface temperature and LCZ classes

Fig. 16.9 shows the differences of LST from the mean value for each LCZ class. In general, there are large variations in LST across LCZ classes while the pattern is similar between the two cities despite the higher differences observed in Hangzhou. The LST of built-up LCZ classes is generally higher than that of the land cover classes, reiterating the high UHI intensity in urban areas. In particular, LCZ 1 (compact high-rise) has the highest LST among the built-up LCZ classes with mean values of 27.3 and 20.8°C for Shanghai and Hangzhou, respectively. LCZ 9 (sparsely built) shows an opposite trend in the two cities with 0.2°C above mean in Shanghai but 1.8°C below mean in Hangzhou. The complex and diverse urban morphology of this LCZ class in YRD is the predominant reason for such an opposite trend since most of the LCZ 9 areas in Hangzhou are located in mountain areas and villages surrounded by farmland and forest. In contrast, LCZ 9 in Shanghai is generally found in suburbs, which experienced rapid urbanization and extensive conversion of land cover.

Lower LST is generally observed in land cover LCZ classes due to the extensive pervious surface in natural land cover. LCZ A exhibits the lowest LST in both cities with mean values of 26.1 and 15.4°C observed in Shanghai and Hangzhou, respectively. However, there are certain inconsistencies in the LST of land cover classes due to the temporal difference in vegetation. Above-mean values were observed in LCZ E (bare rock or paved) in which some of them are concrete paved areas such as an airport and scattered settlements. LCZ G has the highest LST due to the highest heat capacity, which cools off slower than other LCZ classes during nighttime.

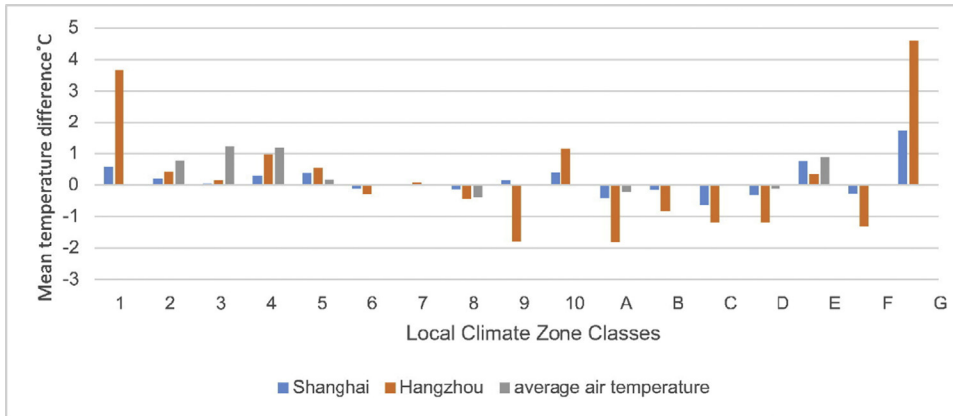


FIGURE 16.9

Temperature differences (°C) from mean LST for each LCZ class.

3.5 Representation of urban morphology of the YRD cities

3.5.1 Regional level

The LCZ maps produced by using the improved WUDAPT methodology were found to be representative of the urban morphology at both city and regional scales. The urban areas in the YRD megaurban region can be classified into four urban agglomerations since the urban morphology is similar with no remarkable delineations among the cities within the agglomerations (Fig. 16.10). Region A is comprised of Shanghai municipality and the surrounding Kunshan in Suzhou and Nantong. The dominant land use in this area is urban and built-up areas with much commercial activity. The urban sprawl of the cities in the region has expanded beyond their administrative boundaries. It has the highest level of urbanization among the four regions, and the urban areas are extremely concentrated and compacted, merging into a large spatial agglomeration. Region B is the Suzhou–Wuxi–Changzhou urban agglomeration to the west of Shanghai. The built-up areas in this region are mainly industrial and commercial. A high level of urbanization is being experienced in this region, and they are likely to develop into a megalopolis in the future.

On the other hand, Region C, located in Hangzhou Bay including cities such as Hangzhou, Shaoxing, and Ningbo, has expanded closely to one another along the coast and contains most of the compact commercial areas. In the north of the YRD megaurban region, Region D consists of Nanjing, Zhenjiang, and Yangzhou, with Nanjing as the center of urban development. The urban area is relatively sparse and smaller than the previous three regions in terms of the size of the city. The urban sprawl of the cities in this region is relatively independent and has not spread together. Due to the rapid economic development in the YRD megaurban region, these four regions are expected to merge and form a megalopolis in the future.

3.5.2 City level

Despite the merging trend in the YRD megaurban region, cities exhibit their characteristics in urban morphology due to their corresponding rates and scenarios of urban development. In Shanghai

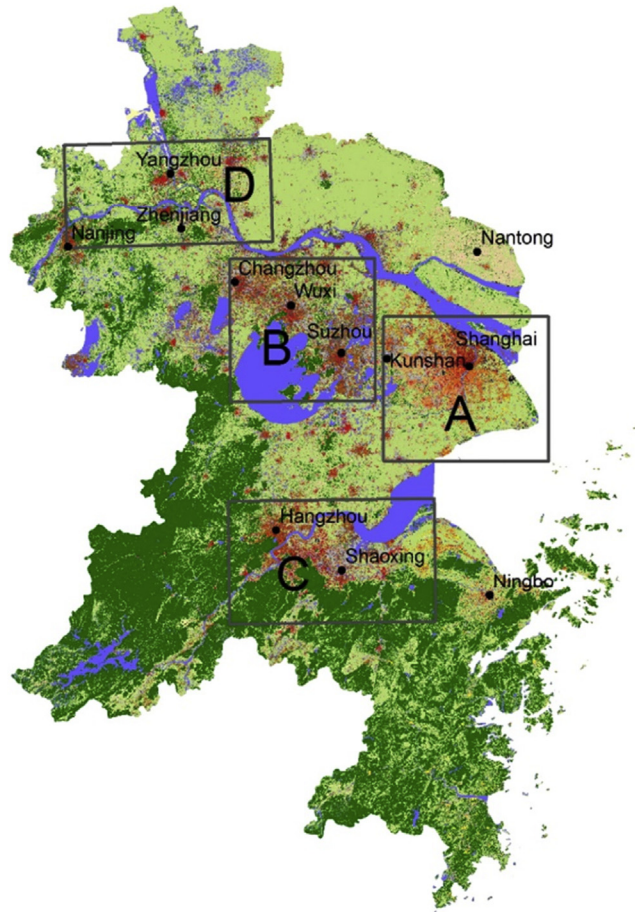


FIGURE 16.10

Urban agglomerations identified in the YRD megarban region.

municipality, LCZ 1 dominates since buildings, especially those in commercial areas, are high-rise and the urban areas are merging into a larger metropolis. In contrast, newly developed districts such as Pudong and Baoshan are well regulated with homogeneous urban morphology. Downtown areas such as the Changning district are more irregular in size and urban form since they are at the early stage of urban development.

Cities at the subprovincial level such as Nanjing and Hangzhou have fewer built-up areas than Shanghai municipality. High-rise buildings and CBDs are generally sparsely located in the city center and often mixed with mid-rise buildings. The block size is usually around 300 m. For prefecture-level cities such as Wuxi and Yangzhou, residential areas dominate and are mostly classified into LCZ 4 and 5. The blocks in these cities are relatively small and disperse with a block size of less than 100 m. The

land use is highly mixed in these cities, and the length of land with homogeneous urban morphology is only around 70–80 m.

Small building blocks mixed with dominant LCZ classes cause problems in selecting training samples from Google Earth, which affects the accuracy of LCZ mapping using the WUDAPT method. In this study, it was found that training samples with a size larger than 100 m² improved mapping results since they provide sufficient information for the classification. On the other hand, the sample with an area less than 100 m² cannot cover one pixel of the Landsat image so the chance of generating an erroneous classification is considerably increased. It is also likely to cause pixel mixing due to uncertainties about the location of the different physical landscapes. However, large samples of homogeneous urban morphology were absent in some cities such as Wuxi, leading to poor mapping results when they were applied to satellite images of 100 m resolution. To improve the mapping result, the small samples and the original Landsat data of 30 m resolution were used for classification. Thus, the Landsat data can better represent the spectral information of the samples and the classification accuracy has therefore been improved. Subclassification of the mix of LCZ types can also help improve the mapping result.

3.6 Implications for urban planning

As the LCZ classification scheme is based on the impact of urban morphology on temperature variation in the city, the LCZ maps can indicate the spatial distribution of the UHI phenomenon, which contributes to more climate-sensitive urban planning. The LCZ map visualizes the spatial characteristics so urban planners and architects can better understand the thermal environment in the decision-making process. Also, the LST characteristics of LCZ classes are helpful to minimize the impacts of urbanization by using urban vegetation and land use planning.

A more severe UHI phenomenon was found in the central and southern parts of the YRD mega-urban region due to the higher level of urban development. Frequent communications between the cities in this part of the region facilitate the emergence of these cities into a megalopolis. Therefore, more careful planning strategies are required for future urban development concerning UHI mitigation. For the dense urban areas in Shanghai, Hangzhou, and Nanjing, further urban development should be avoided or carefully designed to alleviate the high temperature. Green patches with low UHI intensity can also be strategically used to effectively mitigate the UHI phenomenon. For areas with high UHI, it is also important to improve the thermal environment through measures such as efficient energy use, building materials, and other ecological measures.

The urban areas of prefecture-level cities such as Wuxi and Suzhou are sparsely distributed. Hotspots of the cities have sprawled from city center to urban fringe and suburban areas while local hotspots emerge in new towns where a large area of vegetation was converted to impervious surface cover. It suggests that urban development in these areas should be carefully planned and designed, for example, providing open space, preserving urban greenery, and enhancing ventilation. These measures are able to provide a cooling effect to mitigate the UHI intensity in these areas.

The extensive industrial zones in the YRD megaurban region such as Baoshan district in Shanghai and Hangzhou Bay also exhibit high LST and worsen the thermal environment. Further measures should be considered to not only limit the building density but also restrict the anthropogenic heat release of the industrial area. Natural land covers such as green space (LCZ A–D) and open space

(LCZ E and F) are beneficial to the surrounding areas. Low building density is therefore preferred to maximize the cooling effect and prevent any blockage of ventilation from these areas.

4. Discussions and implementations

Not only is the LCZ map suitable for formulating urban planning strategies to mitigate UHI by analyzing the intraurban UHIs, but it has also been proven helpful in improving the local climate via various applications, such as air pollution assessment, heatwave estimation, urbanization projection.

Our research team has already analyzed the impact of urban land cover on air pollution prediction, particularly the particulate matter that $<2.5 \mu\text{m}$ in aerodynamic diameter (PM_{2.5}) by adopting LCZ (Shi et al., 2019). PM_{2.5} is recognized as one of the major pollutants that reduce air quality and increase health burden. This study focused on identifying the influential landscape categories/types from LCZ that affect PM_{2.5} concentration levels in Hong Kong, a high-density city in the PRD region. The results show that a Geographically Weighted Regression (GWR) model, which only incorporates five land use/landscape categories from the LCZ map, can explain 62% of variations in PM_{2.5} without using any traffic-related variables or data in the emission inventory. The understanding of the impact of urban land cover on PM_{2.5} can facilitate planning strategies in terms of mitigating air pollution. This finding can also be particularly useful to the urban air quality assessment in areas without detailed emission inventory or monitoring data since the LCZ map can be retrieved using open data. The method can also be applied to global cities with a globally standardized WUDAPT level 0 database, contributing to the global PM_{2.5} predictions.

The urban land cover properties from the LCZ maps have also been used to predict the distribution of heatwaves in the PRD region. Our research team estimated the spatial pattern of heatwaves in the PRD region at 100 m spatial resolution based on the LCZ maps, observational weather records, and a random forest classifier (Shi et al., 2021). The results show that the methodology can be used to estimate the spatial pattern of heatwaves using open data and provide a basis for policies and decision-making. The spatial pattern of heatwaves is essential for providing corresponding weather services, formulating strategies to adapt to climate change, and undertaking thermal sanitation actions.

Understanding future urbanization is essential for coping with the negative impacts of climate change. There are frequent transitions among different urban land covers and thus altering surface properties, especially for rapidly developing Chinese megaurban regions. To facilitate climate prediction with these changing attributes, the research team proposes a new framework that uses a cellular automata (CA) land use/land cover change (LCLUC) model to predict future LCZ maps of the PRD region (Huang et al., 2021). Unlike most existing LCLUC studies that treat urban areas as homogeneous, our work is the first attempt to simulate the complex conversion between low, medium, and high-rise urban land covers defined in the LCZ scheme. Based on the LCZ maps of the PRD region in 2009 and 2014 as well as the LCLUC rules discovered by data mining technology, we applied the 2014 forecast on the 2009 LCZ map of the CA model. The comparison between the LCZ prediction map and the observed map in 2014 yielded a kappa coefficient of 0.77, with a global accuracy of 82%. Our results show that the combination of the LCZ scheme and LCLUC modeling has the potential to capture changes in intraurban structure and provide the necessary input datasets for urban climate prediction.

5. Conclusions

The development of megarban regions is a national strategy that focuses on future urban development in China. This study uses the LCZ scheme and LST to analyze the intraurban UHI effect of the YRD and PRD megarban region. Although the concept of the LCZ classification scheme is based on measurements of air temperature, LST was found to be associated with LCZ classes and suitable for intraurban UHI analysis. In the PRD region, urbanization is found to comprise transformation from natural land covers to built types, densification, and vertical enhancement of existing urban structures. Second, the land surface was warming with a speed of up to >0.3 K/year, and the hot area expanded in accordance with urbanized areas in the PRD region during the study period. The expansion of LCZ built types has led to a significant LST increase. In particular, the large extension of LCZ 8 (large low-rise) and LCZ 6 (open low-rise) results in a high LST increase. LCZ 4 (open high-rise) and LCZ 8 (large low-rise) are the dominant LCZ types in the high SUHI zones. In the YRD region, built-up LCZ classes generally exhibit higher LST than land cover LCZ classes. LCZ 1 and 10 have the highest LST among the built-up classes in the two cities while vegetation (LCZ A-D) has the lowest among all classes. Inconsistencies in LST variations were found in LCZ 9, A, B, and C due to the highly variable urban morphology and the temporal variations in vegetation.

The findings can show researchers a new way of extracting the detailed urban and land use data from open-sourced satellite data. Owing to the diverse LCZ built types, this study can investigate the intraurban UHI difference in the two megarban regions, instead of the rough one urban category or two to three urban classes (low/medium/high density) applied by previous studies. The findings can help urban planners and urban climate researchers better understand the influence of urban morphology (i.e., LCZ classes) on local climatic conditions. Thus, land use planning and management play a crucial role in SUHI reduction under climate change adaptation. Proper and reasonable distribution of LCZ with lower surface temperatures is advisable to mitigate the influence of UHI during the process of urban development. The findings of this study can also help researchers to better understand the influence of LCZ on local climate variations for other Chinese megarban regions and global cities. Results also support air quality assessment, future urbanization projection, heatwave studies, and numerical models for climate change studies. However, limited by the resolution of freely available remote sensing images (tens of meters to hundreds of meters), the LCZ-based SUHI investigation focuses on the local scale, microscale exploration of the UHI effect needs to be conducted by other fine-scale numerical modeling or mobile measurement.

References

- Allen, M.R., Barros, V.R., Broome, J., Cramer, W., Christ, R., Church, J.A., Edenhofer, O., 2014. IPCC Fifth Assessment Synthesis Report-Climate Change 2014 Synthesis Report.
- Bechtel, B., Daneke, C., 2012. Classification of local climate zones based on multiple earth observation data. *IEEE J. Sel. Top. Appl. Earth Obs. Rem. Sens.* 5 (4), 1191.
- Bechtel, B., Alexander, P.J., Böhner, J., Ching, J., Conrad, O., Feddema, J., Stewart, I., 2015. Mapping local climate zones for a worldwide database of the form and function of cities. *ISPRS Int. J. Geo-Inf.* 4 (1), 199–219.

- Bechtel, B., Alexander, P.J., Beck, C., Böhner, J., Brousse, O., Ching, J., Xu, Y., 2019. Generating WUDAPT Level 0 data — current status of production and evaluation. *Urban Climat.* 27, 24–45. <https://doi.org/10.1016/j.uclim.2018.10.001>.
- Breiman, L., 2001. Random forests. *Mach. Learn.* 45 (1), 5–32.
- Ching, J., Mills, G., Bechtel, B., See, L., Feddema, J., Wang, X., Neophytou, M., 2018. World Urban Database and Access Portal Tools (WUDAPT), an Urban Weather, Climate and Environmental Modeling Infrastructure for the Anthropocene. *Bulletin of the American Meteorological Society*, 2018.
- Clinton, N., Gong, P., 2013. MODIS detected surface urban heat islands and sinks: global locations and controls. *Remote Sens. Environ.* 134, 294–304. <https://doi.org/10.1016/j.rse.2013.03.008>.
- Dong, L., Jiang, Z., Shen, S., 2014. Urban heat island change and its relationship with urbanization of urban agglomerations in Yangtze River Delta in past decade. *Transact. Atmos. Sci.* 37 (2), 146–154.
- Government of Guangdong Province, 2010. Pearl River Delta Urban and Rural Integration Planning. Guangzhou: Government of Guangdong Province.
- Heinl, M., Hammerle, A., Tappeiner, U., Leitinger, G., 2015. Determinants of urban–rural land surface temperature differences — a landscape scale perspective. *Landsc. Urban Plann.* 134, 33–42. <https://doi.org/10.1016/j.landurbplan.2014.10.003>.
- Hong Kong Observatory, 2015. Hong Kong in a Warming World. Hong Kong Observatory, Hong Kong.
- Huang, K., Leng, J., Xu, Y., Li, X., Cai, M., Wang, R., Ren, C., 2021. Facilitating urban climate forecasts in rapidly urbanizing regions with land-use change modeling. *Urban Clim.* 36, 100806.
- Lambin, E.F., 1997. Modelling and monitoring land-cover change processes in tropical regions. *Prog. Phys. Geogr.* 21 (3), 375–393. <https://doi.org/10.1177/030913339702100303>.
- Mallick, J., Kant, Y., Bharath, B.D., 2008. Estimation of land surface temperature over Delhi using Landsat-7 ETM+. *J. Ind. Geophys. Union* 12 (3), 131–140.
- McCarthy, M.P., Best, M.J., Betts, R.A., 2010. Climate change in cities due to global warming and urban effects. *Geophys. Res. Lett.* 37 (9).
- Murdiyarto, D., 2000. Adaptation to climatic variability and change: asian perspectives on agriculture and food security. *Environ. Monit. Assess.* 61 (1), 123–131. <https://doi.org/10.1023/a:1006326404156>.
- National Development, Reform Commission, 2016. Regional Planning of Yangtze River Delta Beijing, China (Retrieved from).
- Oke, T.R., 1973. City size and the urban heat island. *Atmos. Environ.* 7 (8), 769–779. [https://doi.org/10.1016/0004-6981\(73\)90140-6](https://doi.org/10.1016/0004-6981(73)90140-6).
- Peng, S.S., Piao, S.L., Ciais, P., Friedlingstein, P., Otle, C., Bréon, F.o.-M., Myneni, R.B., 2011. Surface urban heat island across 419 global big cities. *Environ. Sci. Technol.* 46 (2), 696–703.
- Qian, L.X., Ding, S.Y., 2005. Impacts of land use and cover change on land surface temperature in the Zhujiang delta. *Acta Geograph. Sin.* 60 (5).
- Santamouris, M., Cartalis, C., Synnefa, A., Kolokotsa, D., 2015. On the impact of urban heat island and global warming on the power demand and electricity consumption of buildings—a review. *Energy Build.* 98, 119–124. <https://doi.org/10.1016/j.enbuild.2014.09.052>.
- Shanghai Municipal Statistics Bureau, 2011. Shanghai Statistical Yearbook 2000–2011. China Statistics Press, Beijing.
- Shi, Y., Ren, C., Lau, K.K.L., Ng, E., 2019. Investigating the influence of urban land use and landscape pattern on PM_{2.5} spatial variation using mobile monitoring and WUDAPT. *Landsc. Urban Plann.* 189, 15–26.
- Shi, Y., Ren, C., Luo, M., Ching, J., Li, X., Bilal, M., Ren, Z., 2021. Utilizing world urban database and access portal tools (WUDAPT) and machine learning to facilitate spatial estimation of heatwave patterns. *Urban Clim.* 36, 100797.
- Statistics Bureau of Guangdong Province, 2001. Guangdong Statistical Yearbook. China Statistics, Beijing.
- Statistics Bureau of Guangdong Province, 2011. Guangdong Statistical Yearbook. China Statistics, Beijing.

- Stewart, I.D., Oke, T.R., 2012. Local climate zones for urban temperature studies. *Bull. Am. Meteorol. Soc.* 93 (12), 1879–1900. <https://doi.org/10.1175/bams-d-11-00019.1>.
- The Central Committee of the Communist Party of China and the State Council (CCCPC & SC), 2014. National Plan on New Urbanization 2014–2020. <http://www.gov.cn/zhuanti/xxczh>.
- Tian, L., Li, Y., Yan, Y., Wang, B., 2017. Measuring urban sprawl and exploring the role planning plays: a shanghai case study. *Land Use Pol.* 67, 426–435.
- Voogt, J.A., Oke, T.R., 2003. Thermal remote sensing of urban climates. *Remote Sens. Environ.* 86 (3), 370–384. [https://doi.org/10.1016/S0034-4257\(03\)00079-8](https://doi.org/10.1016/S0034-4257(03)00079-8).
- Wang, C., Liu, J., 1982. The climate of the city of Hangzhou. *Acta Geograph. Sin.* 37, 164–173.
- Wang, W., Zheng, G., 2013. 2013 Green Book of Climate Change. Social Sciences and Academic Press.
- Weng, Q., 2001. A remote sensing?GIS evaluation of urban expansion and its impact on surface temperature in the Zhujiang Delta, China. *Int. J. Rem. Sens.* 22 (10), 1999–2014. <https://doi.org/10.1080/713860788>.
- Zhang, H., Qi, Z.F., Ye, X.Y., Cai, Y.B., Ma, W.C., Chen, M.N., 2013. Analysis of land use/land cover change, population shift, and their effects on spatiotemporal patterns of urban heat islands in metropolitan Shanghai, China. *Appl. Geogr.* 44, 121–133.
- Zhao, L., Lee, X.H., Smith, R.B., Oleson, K., 2014. Strong contributions of local background climate to urban heat islands. *Nature* 511 (7508), 216.